

INTERACTION OF LASER RADIATION WITH MATTER. LASER PLASMA https://doi.org/10.1070/QEL16784

Uniformity simulation of multiple-beam irradiation of a spherical laser target with the inclusion of radiation absorption and refraction

N.N. Demchenko, S.Yu. Gus'kov, N.V. Zmitrenko, V.B. Rozanov, R.V. Stepanov

Abstract. **We consider the physicomathematical model for the simulation of the angular laser flux distribution in a spherical target with the inclusion of radiation refraction in the corona. The irradiation uniformity is simulated using the target irradiation scheme on a megajoule multiple-beam laser facility. Calculations are made of the time-dependent angular distribution of absorbed flux and of the angular distribution of the time-integrated characteristic – the absorbed energy with allowance for the temporal shape of laser pulses – as well as of the time dependence of absorption efficiency. Different versions of target irradiation are considered. Under conventional irradiation it is assumed that the axes of all laser beams of equal energy pass through the target centre and the irradiation nonuniformity is due to its geometry only. Also examined are three unconventional irradiation versions: when there is a small spread of beam energies, when the target is displaced from the common beam pointing centre, and when the beam axes have small random deviations from the target centre. It is shown that the nonuniformity of the angular distribution of absorbed flux is greatest when the target is displaced from the beam pointing centre.**

Keywords: *target irradiation nonuniformity, absorption and refraction of radiation, angular distribution of absorbed flux, beam energy spread, beam pointing errors, target displacement from beam pointing centre.*

1. Introduction

At present, different target compression and ignition schemes are under consideration in laser fusion research (for a review of the schemes, see, for instance, Refs [1, 2]). One of the schemes, which permits the most efficient use of laser energy for the compression and heating of a thermonuclear target, is the scheme of direct target irradiation by a multitude of laser beams. To achieve a close-to-spherically symmetric target compression, the number of beams should be rather high and the target-irradiating beam directions must somehow be uniformly distributed in space. Considered early in the research was the irradiance problem of the spherical target irradiated by the set of laser beams [3–5]. These works were primarily aimed at studying the effect of different irradiation geometries on the irradiance symmetry. Scannapieco and Brysk [6] considered the uniformity of laser energy deposition in a spherically symmetric plasma corona assuming that the characteristic plasma nonuniformity length $L_{cr} = (d\varepsilon'/dr|_{r_{cr}})^{-1}$ is much shorter than the critical radius r_{cr} (here, $\varepsilon' = \varepsilon'(r) = 1 - \omega_p^2(r)/\omega^2$; ω_p and ω are the plasma and laser frequencies; $\varepsilon'(r_{cr}) = 0$). As shown in Ref. [7], for $L_{cr}/r_{cr} \ll 1$ it is possible to neglect refraction and consider the problem of critical surface irradiation by introducing a factor to take into account the efficiency of absorption.

The authors of Ref. [7] considered a model which described the angular distribution of absorbed laser flux in a spherically symmetric plasma corona with the inclusion of radiation refraction. The optical axis of a laser beam was assumed to pass through the target centre and the intensity dependence was assumed to be axially symmetric over the beam cross section. Then, the function $W_1(\mu, t)$, which describes the angular distribution of the absorbed flux for one laser beam (a single-beam function), depends only on $\mu = \cos\theta$ and time t, where θ is the spherical angle measured from the optical axis of the beam (the origin of the reference frame is at the target centre). The problems arising in the selection of the model for calculating function $W_1(\mu, t)$ were considered in Ref. [7]. As shown in Ref. [7], when the laser energy deposition in the corona is integrated over the radius and the dependence on μ remains, for $\mu = 1$ the greatest contribution to this function is made by the vanishing energy deposition with the radius tending to infinity ($r \to \infty$). Specifically, consider a ray segment of length Δl. The flux fraction ΔQ_a related to this ray and absorbed over a length Δl tends to zero for $r \to \infty$, since the plasma density tends to zero. However, the solid angle $\Delta\Omega = \Delta\mu\Delta\varphi$, which corresponds to the ray element Δl, also tends to zero, because there vanishes the angle $\Delta\mu$, at which the element Δl is seen from the target centre. In this case the ratio $\Delta Q_a/\Delta\Omega$ has a maximum at infinity.

The model of calculating the function W_1 considered in Ref. [7] consisted in that the real dependence $\Delta Q(l)$ (l is the coordinate along the ray) of the ray-related differential flux was replaced by a step function with a step from the incident flux ΔQ_0 to the flux ΔQ_r emerging from the plasma at a ray point l^*, prior to which a half of the radiation flux is absorbed, i.e. $(\Delta Q_0 - \Delta Q^*)/\Delta Q_0 = \delta_a/2$, where $\delta_a = (\Delta Q_0 - \Delta Q_r)/\Delta Q_0$ is the fraction absorbed. This is the model of δ-like flux absorption on the surface consisting of points l^* on the rays. This model makes it possible to avoid the contribution made to the function W_1 by the weak absorption away from the critical

N.N. Demchenko, V.B. Rozanov, R.V. Stepanov P.N. Lebedev Physical Institute, Russian Academy of Sciences, Leninsky prosp. 53, 119991 Moscow, Russia; e-mail: demch@lebedev.ru;
S.Yu. Gus'kov P.N. Lebedev Physical Institute, Russian Academy of Sciences, Leninsky prosp. 53, 119991 Moscow, Russia; National Research Nuclear University 'MEPhI', Kashirskoe sh. 31, 115409 Moscow, Russia;
N.V. Zmitrenko M.V. Keldysh Institute of Applied Mathematics, Russian Academy of Sciences, pl. Miusskaya 4, 125047 Moscow, Russia

Received 13 July 2018; revision received 5 September 2018
Kvantovaya Elektronika **49** (2) 124–132 (2019)
Translated by E.N. Ragozin

surface near the optical axis ($\mu \approx 1$). However, in the perpendicular direction to the optical axis ($\mu \approx 0$) this model is not always applicable. Away from the critical surface the family of points l^* falls on a straight line passing through the target centre perpendicular to the optical axis. This has the effect that the greatest contribution to function W_1 in the vicinity of $\mu \approx 0$ can be made by the distant low-density plasma. On the other hand, the transverse beam size, unlike the longitudinal one, is limited by values of the order of the critical radius, and this feature is 'clipped' by the transverse beam profile. However, when the beam radius is varied over a wide range and its effect on the angular distribution of absorbed flux is investigated, the contribution of remote domain may lead to the results that inadequately show the distribution in the domain of the main energy deposition. In reality, in the vicinity of $\mu \approx 0$ it is required to take into account the distributed nature of absorption.

The aim of our work is to generalise the model for calculating function W_1 so as to take into account the distribution of the energy deposition along the ray. Furthermore, we consider the cases when the optical beam axis does not pass through target centre and deviates to some extent from it (a miss). In this case, the one-beam function W_1 does not possess axial symmetry despite the axial symmetry of the incident beam intensity.

The nonuniformity of absorbed laser flux distribution has the effect that the ablation pressure on the target ablation surface also becomes nonuniform. However, the ablation pressure depends not only on the laser flux density, but also on the plasma density at which the bulk of absorption takes place. In the stationary corona model [8, 9], for instance, it depends on the critical density (or the wavelength of laser radiation), whereby there occurs the δ-like energy deposition from the laser flux. When the absorption and refraction of rays in the corona are taken into account, the peak of energy deposition is in the subcritical plasma and not on the critical surface. In this case, the plasma density in the domain of peak energy deposition depends on the angle μ. Apart from the single-beam distribution function $W_1(\mu, t)$ it is therefore necessary to consider the single-beam function $\rho_1^*(\mu, t)$ for the characteristic density, whereby the bulk of absorption of the laser flux takes place.

2. Absorbed laser flux distribution function over the solid angle and characteristic plasma density at which energy deposition takes place

At first we consider the case when the optical beam axes pass through the target centre. The general simulation scheme of the angular distribution of the flux absorbed in the target is as follows. The one-dimensional hydrodynamic RAPID code [10] is used to calculate the angular distribution function $W_1(\mu, t)$ for absorbed laser flux from one laser beam at several prescribed points in time t between the onset of the pulse and the instant of target collapse. Also calculated is the characteristic density function $\rho_1^*(\mu, t)$ (measured in units of the critical density) whereby there occurs absorption of the energy flux of one beam. Then, for a given geometry of target irradiation by a set of beams we calculate the total angular distribution of absorbed flux and energy as well as the angular distribution of the characteristic density at which the energy deposition is greatest (this calculation is performed with a separate code).

Consider the model used for the calculation of W_1 and ρ_1^*. The absorption and reflection of laser radiation of laser radiation in the RAPID code is considered on the basis of the combination of ray and wave approaches. The ray trajectory in the plasma corona is constructed with the inclusion of refraction, and in a small neighbourhood of the turning point of the ray we solve the Maxwell equations for oblique wave incidence on a plane layered plasma for s- and p-polarised wave components. Calculated in the issue are the dependences of the absorption fractions δ_{as} and δ_{ap} for s- and p-polarised radiation on the ray coordinate p in the plane perpendicular to the optical axis. For a beam of parallel rays, p is the impact parameter of the ray. The fraction of resonance absorption is determined by the difference $\delta_{ap} - \delta_{as}$. Under the conditions of hydrodynamic target compression mode the total resonance absorption fraction turns out to be small, since $L_{cr}/\lambda \gg 1$, where λ is the wavelength of laser radiation. In this case, only a very small fraction of the laser flux confined near the optical axis (the resonance absorption fraction is given below) participates in the resonance absorption, and so only the inverse bremsstrahlung mechanism may be considered in the simulation of absorbed flux uniformity.

Consider the energy deposition model for the calculation of absorbed flux nonuniformity. We replace the real distributed energy deposition along a ray by a model one with the use of the following scheme. At a ray point l^*, ahead of which a half of the radiation flux is absorbed, the derivative $[\mathrm{d}(\Delta Q)/\mathrm{d}\mu]^*$ is calculated along the ray. We replace the dependence $\Delta Q(\mu)$ in the neighbourhood of point l^* by a linear dependence with the slope equal to the calculated derivative to determine the characteristic angular dimension $\Delta\mu_l = \Delta Q_a/[\mathrm{d}(\Delta Q)/\mathrm{d}\mu]^*$ over which the absorbed flux $\Delta Q_a = \Delta Q_0 - \Delta Q_r$ is distributed in the motion along the ray. Furthermore, the incident flux $\Delta Q_0 = 2\pi I(p)p\,\mathrm{d}p$, where $I(p)$ is the beam intensity, at point l^* has its own angular dimension $\Delta\mu^*$, because the rays with impact parameters p_i and $p_{i+1} = p_i + \Delta p_i$ have different μ_i^*, and consequently $\Delta\mu_{i+1/2}^* = \mu_i^* - \mu_{i+1}^*$. The total angular dimension over which the absorbed flux ΔQ_a is absorbed is written as the sum $\Delta\mu = \Delta\mu_l + \Delta\mu^*$. The term $\Delta\mu_l$ is absent in the δ-like energy deposition model and $\Delta\mu = \Delta\mu^*$. The function $W_1(\mu)$ summarised over all differential incident fluxes ΔQ_0 is found by integration:

$$W_1(\mu) = 2\pi \int_0^{p_{\max}} \frac{1}{\Delta\mu} \eta[(\mu - \mu_1)(\mu_2 - \mu)]\, \delta_{as}(p) I(p) p\, \mathrm{d}p, \quad (1)$$

where η is the Heaviside function ($\eta(x) = 0$ for $x < 0$, $\eta(x) = 1$ for $x \geqslant 0$); $\mu_1 = \mu^* + \Delta\mu/2$; $\mu_2 = \mu^* - \Delta\mu/2$; μ^*, μ_1, μ_2 and $\Delta\mu$ are function of parameter p. In expression (1) we omitted the time t for simplicity of notation. In reality, as noted above, integrals (1) are calculated for a sequence of points in time and all quantities that appear in the integrand are time-dependent. For the characteristic density ρ_1^* it would be natural to take the density at the ray point l^*, at which $\mu = \mu^*$. Thus we obtain the single-beam characteristic density function $\rho_1^*(\mu, t)$, at which there occurs the main absorption due to inverse bremsstrahlung mechanism.

When the function $W_1(\mu)$ is known, the total energy deposition for N beams is determined by summing at a given point (θ, φ) the energy depositions of all beams, which requires calculating the cosines of the angles between the direction (θ, φ) and the optical beam axes (θ_n, φ_n):

$$\mu_n(\theta,\varphi) = \sin\theta_n\cos\varphi_n\sin\theta\cos\varphi + \sin\theta_n\sin\varphi_n\sin\theta\sin\varphi + \cos\theta_n\cos\theta. \quad (2)$$

The angular distribution function of N beams

$$W(\theta,\varphi) = \sum_{n=1}^{N} W_1(\mu_n(\theta,\varphi)). \quad (3)$$

Unlike the energy deposition, the characteristic densities are not summed. Taken for $\rho^*(\theta,\varphi)$ is the density $\rho_1^*(\mu_n(\theta,\varphi))$ of the beam which makes the greatest contribution to the energy deposition, i.e. the beam whose term in the sum (3) is greatest.

We note that expression (3) sums the beam intensities. In reality, even in one beam the wavefront may be partly coherent, and in this case there appears correlation between the partly coherent portions of the wavefront, which gives rise to narrow spikes in the intensity distribution in the focal plane. Here we consider only the statistically average intensity distributions, which overlap in the target irradiation by a large number of beams to give an energy distribution close to the spherically symmetric one. An investigation of the problem of the effect of intensity spikes does not call for the summation over all beams. This is a separate problem of whether a sharp intensity spike will have time to be smooth out in the target or how to vary these spikes in time and space to smooth out their effect in the corona without a significant pressure transfer to the target shell under acceleration. When the focal spot size far exceeds the diffraction limit $\lambda(F/D)$, where F is the focal distance and D is the beam aperture diameter, this signifies that the size d_{coh} of coherent portion of the wavefront is much shorter than D. In this case, for an elementary beam one has to consider the beam of aperture d_{coh} and perform averaging of the single-beam distribution function over the entire aperture of the laser beam (the averaging procedure was considered in Ref. [7]).

Now let us dwell on the case when the optical beam axis OF passes some distance δ from the target centre (δ is the impact parameter, or axis miss distance) (Fig. 1). This case emerges in two problems: first, when each of the beam axes exhibits a random miss distance δ_n relative to the target centre and, second, when all axes converge at one pointing centre but the target is somewhat displaced from the pointing centre. We draw a new axes O′F through the focal point F and the target centre, as shown in Fig. 1. The plasma density and temperature distributions about the O′F axis possess axial symmetry, and therefore the ray paths in the plasma are also axially symmetric around this axis. The dependence of energy deposition on the angle φ' measured from the O′F axis appears, because in this coordinate system the incident beam intensity is not axially symmetric and depends on r' and φ'. The angle φ' is measured from the perpendicular to the O′F axis drawn in the plane OFO′ (Fig. 1). When the beam intensity distribution relative to the OF axis

$$I(r) = I_0\exp\left[-\left(\frac{r}{A}\right)^p\right] \quad (4)$$

(r is the distance from the OF axis and A is the characteristic beam radius in the plane of the focusing device), the dependence $I'(r',\varphi')$ relative to the O′F axis is obtained from formula (4) by expressing r in terms of r' and φ'. The dependence $r(r',\varphi')$ is found from the triangle two sides of which, r' and b, form the angle φ' (Fig. 1) ($b = F\delta/\Delta$, Δ is the focal spot displacement from the target centre):

$$r = \sqrt{(r' - b\cos\varphi')^2 + (b\sin\varphi')^2}. \quad (5)$$

The single-beam absorbed flux distribution function is calculated similarly to the case when the beam axis passes through the target centre (1), with the inclusion of the dependence of incident intensity on the φ' angle:

$$W_{1n}(\mu',\varphi') = \int_0^{p'_{\max}} \frac{1}{\Delta\mu'}\eta[(\mu'-\mu'_1)(\mu'_2-\mu')] \times \delta_{\mathrm{as}}(p')I'_n(p',\varphi')p'\mathrm{d}p'. \quad (6)$$

All quantities in the integrand are the same as in expression (1). When the differential flux $I'_n(p',\varphi')p'\mathrm{d}p'\mathrm{d}\varphi'$ is divided by the solid angle $\Delta\mu'\mathrm{d}\varphi'$, the factor $\mathrm{d}\varphi'$ cancels out. Since the dependence of the intensity $I'_n(p',\varphi')$ contains the optical axis miss distance δ_n for the nth beam and, consequently, the quantity b_n should appear in formula (5) for the nth beam (the miss distances are different for all beams), each beam has its own single-beam distribution function (6) [this is indicated with subscript n in expression (6)]. Of interest usually are short miss distances δ_n, which are much smaller than the characteristic beam radius at the target, because the beam radius and the target radius should be close. In this case, the amount of calculations in expression (6) may be greatly reduced. Considering b in expression (5) as a small parameter and using formula $\sqrt{1-x} \approx 1 - x/2$, which holds good for small x, expression (5) may be rearranged to the following form:

$$r - r_0 = \frac{r'b}{\sqrt{r'^2 + b^2}}\cos\varphi', \quad (7)$$

where $r_0 = r_0(r', b) = \sqrt{r'^2 + b^2}$. We replace the intensity $I(r)$ in the neighbourhood of point r_0 with the linear function of the form

$$I(r) \approx I(r_0) + \left.\frac{\mathrm{d}I}{\mathrm{d}r}\right|_{r_0}(r - r_0), \quad (8)$$

to obtain

$$I'(r',\varphi',b) = I(r_0(r',b)) + \left.\frac{\mathrm{d}I}{\mathrm{d}r}\right|_{r_0}\frac{r'b}{\sqrt{r'^2 + b^2}}\cos\varphi'. \quad (9)$$

As follows from expression (9), for small value of parameter b the single-beam function (6) contains a term proportional to $\cos\varphi'$. Furthermore, this term depends linearly on parameter b

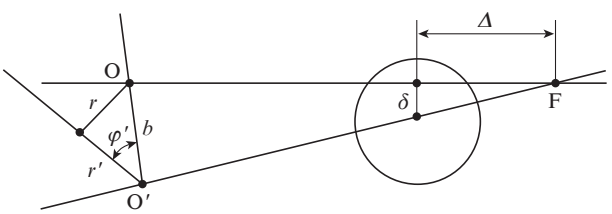

Figure 1. Diagram explaining the introduction of a new optical axis in the case of a small miss of the laser beam relative to the target centre.

in the neighbourhood of point $b = 0$. The algorithm of calculating $W_{1n}(\mu',\varphi')$ in this case is therefore as follows. Three functions are calculated: $W_0(\mu')$ is the function for $b = 0$ (this the axially symmetric case, when $\mu' = \mu$); $W_{B0}(\mu')$ is the function for the greatest parameter $b_{\max} = B$ and $\varphi = 0$; and $W_{B\pi}(\mu')$ is the function for $b_{\max} = B$ and $\varphi = \pi$. For other values of b_n and φ' the function W_{1n} is calculated by the formulas

$$W_{1n} = W_0(b_n)\cos^2\frac{\varphi'}{2} + W_\pi(b_n)\sin^2\frac{\varphi'}{2}, \tag{10}$$

$$W_0(b_n) = W_{00} + (W_{B0} - W_{00})\frac{b_n}{B}, \tag{11}$$

$$W_\pi(b_n) = W_{00} + (W_{B\pi} - W_{00})\frac{b_n}{B}. \tag{12}$$

The sum function of absorbed flux angular distribution from N beams is written in the form

$$W(\theta,\varphi) = \sum_{n=1}^{N} W_{1n}(\mu'_n(\theta,\varphi),\varphi'_n(\theta,\varphi)), \tag{13}$$

where μ'_n is the cosine of the angle between the direction (θ,φ) considered in the target and the direction of 'corrected' optical axis O′F (Fig. 1); φ'_n is the angle made with the OFO′ plane by the direction (θ,φ) considered in the target (Fig. 1) for nth beam.

3. Simulation of the angular distribution of absorbed laser flux for experimental conditions on a megajoule laser

Calculations were made for the following conditions. A pulse of the second harmonic of Nd-laser radiation has an energy of 2 MJ. The temporal pulse shape is depicted in Fig. 2. The target consists of a 34-μm thick CH shell with an outer radius of 1597 μm and a 150-μm thick DT ice shell adjoining it on the inside. Inside of the shell is a DT gas at a density of 10^{-3} g cm^{-3}. The number of laser beams is equal to 48. The optical beam axes are directed along the generatrices of cones, whose vertices are at the target centre (at the origin) and whose base centres coincide with the Cartesian axes x, y, z. In all, there are six cones arranged with cube symmetry. The cone half-angle is equal to 30°. Each cone comprises eight beams, and the angle $\Delta\varphi$ between the directions at the cone base is equal to 45°. If we consider the cone on the z axis, the angles φ_n relative to the x axis in the (x, y) plane begin with 22.5° and next increase by 45° each relative to the previous one. The beams in the other cones are arranged in a similar way. The beam aperture diameter $D = 80$ cm and the focal distance $F = 660$ cm. The radiation intensity distribution in the target plane (the plane passing through the target centre perpendicular to the optical axis) is as follows:

$$I(r) = I_0\exp\left[-\left(\frac{r}{a}\right)^p\right], \tag{14}$$

where r is the distance from the optical axis and a is the characteristic beam radius. The value of a was varied in the simulations, the ratio a/R (R is the initial target radius) varied from 0.5 to 1.3. We considered a Gaussian beam with $p = 2$ and a super-Gaussian beam with $p = 4$. Since the absorption efficiency depends on the electron temperature in the corona and this temperature depends on the electron thermal conduction flux limiter f, we considered both the case of limited thermal conduction with $f = 0.06$ and the case of Spitzer conductivity (without thermal flux limitation). The electron thermal flux $W_e = W_S W_{\max}/(W_S + W_{\max})$, where W_S is the Spitzer flux; $W_{\max} = fn_eT_ev_{T_e}$; and n_e, T_e and $v_{T_e} = (T_e/m_e)^{1/2}$ are the electron density, temperature and thermal velocity, respectively.

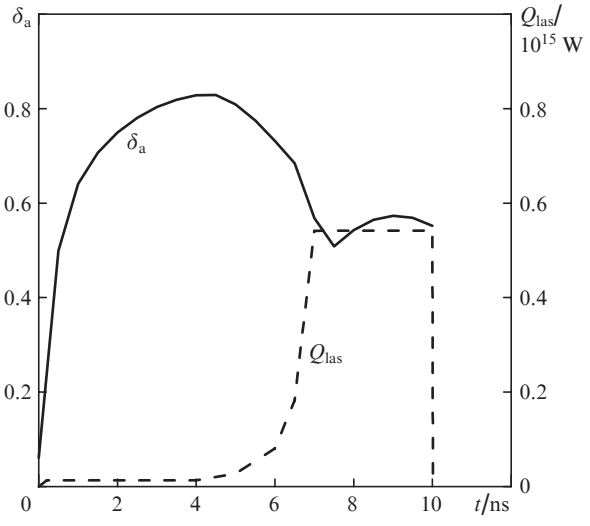

Figure 2. Time dependences of the laser flux Q_{las} and its absorption efficiency δ_a in the plasma corona.

At first we consider the conventional irradiation case, when all beam axes pass through the target centre and all beam energies are equal. Figure 3a shows the distributions $W_1(\mu)$ produced by one beam at different points in time for $p = 2$, $a/R = 1$, and $f = 0.06$. The angle θ ($\mu = \cos\theta$) is measured from the optical beam axis. The distributions are normalised to the peak of the function $W_1(\mu)$. One can see the 'broadening' of the function $W_1(\mu)$ at later points in time. This is due first to a shortening of the critical surface radius in the shell motion towards the centre for an invariable beam radius at the target, and second, to an incident flux redistribution over the beam cross section arising from refraction of the rays in the corona. The refraction is responsible for a lowering of the intensity on the optical axis (in the region $\mu \approx 1$) and for its increase at some distance from the optical axis ($\mu < 1$). This effect was discussed at length in Ref. [7]. Shown in Fig. 3b for the same version are the dependences of the characteristic density ρ_1^*/ρ_{cr} (in units of the critical density) on μ for one beam at different points in time. As is clear in Fig. 3b, the characteristic density, at which there occurs the main energy deposition, is lower than the critical density. This is because the optical thickness of plasma along the rays close to the optical axis ($\mu \approx 1$) is high and the radiation experiences significant absorption prior to the critical density region. This density is especially low at the points in time when the laser intensity is low ($t = 4.5$ ns, Fig. 3b) and, accordingly, the optical thickness near the optical axis is high. For rays distant from the optical axis ($\mu < 1$) the density ρ_1^* is lower than ρ_{cr} due to ray refraction in the corona, since the radiation reaches only the turning point, at which the plasma density is lower than ρ_{cr}.

For the irradiation geometry considered above we calculated the angular distribution function $W(\theta,\varphi,t)$ for the flux absorbed at different points in time as well as the angular distribution for the absorbed energy $E(\theta,\varphi)$ with the inclusion

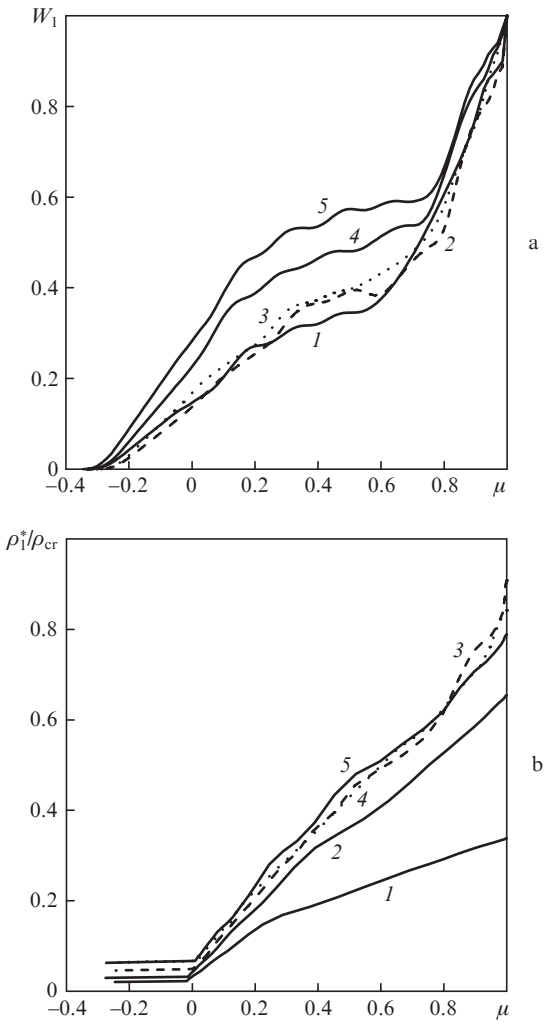

Figure 3. (a) Single-beam angular distribution function for absorbed flux at the time moments (*1*) 6.5, (*2*) 7.5, (*3*) 8.5, (*4*) 9.5, and (*5*) 10 ns, as well as (b) angular plasma density dependences at the ray points prior to which a half of the differential flux is absorbed at the time moments (*1*) 4.5, (*2*) 6.5, (*3*) 7.5, (*4*) 8.5, and (*5*) 9.5 ns; μ is the cosine of the angle measured from the optical axis of the beam.

of the time dependences of the incident laser flux $Q_{las}(t)$ and the absorption fraction $\delta_a(t)$:

$$E(\theta,\varphi) = \int_0^{\tau_{las}} W(\theta,\varphi,t)\, Q_{las}(t)\delta_a(t)\,\mathrm{d}t. \qquad (15)$$

The dependences $Q_{las}(t)$ and $\delta_a(t)$ are plotted in Fig. 2. The functions W and E are so normalised that their values averaged over the entire solid angle of 4π are equal to unity. Figure 4 shows the dependence $E(\theta,\varphi)$. In this case, the degree of uniformity $\eta_E = E_{min}/E_{max}$ is equal to 0.9663 and the difference between the maximum and the minimum of the function $E(\theta,\varphi)$ is $\varepsilon_E \approx 1 - \eta_E = 3.4\%$. The $W(\theta,\varphi,t)$ distributions are of the same shape as the $E(\theta,\varphi)$ distribution, and the degree of uniformity $\eta_W = W_{min}/W_{max}$ varies with time and lies in the range 0.934–0.968. The maxima and minima of the $W(\theta,\varphi,t)$ function move in the plane (θ,φ) with time, with the consequence that the time-integrated value of $E(\theta,\varphi)$ exhibits a higher degree of uniformity.

Figure 5 shows the map of relative densities $D^* = \rho^*/\rho_{cr}$ at which there occurs the greatest energy deposition under target

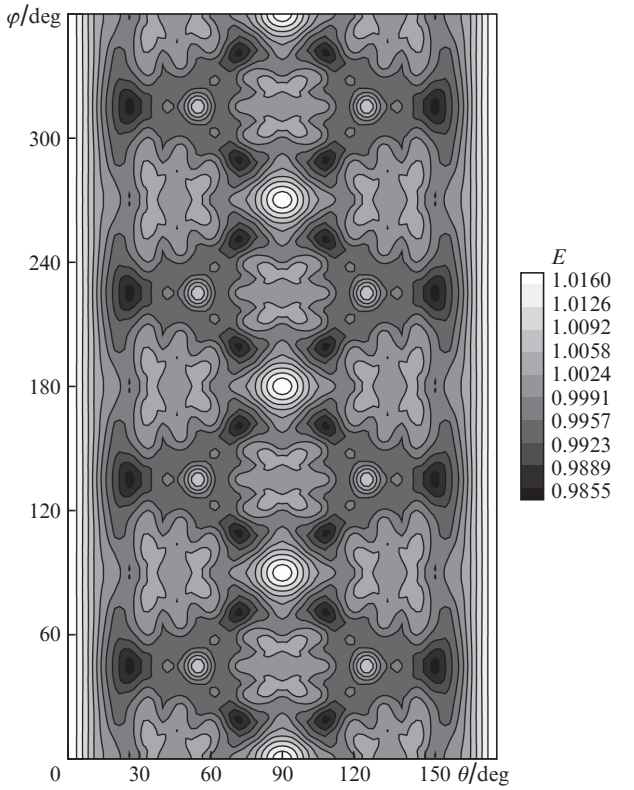

Figure 4. Angular distribution function for the energy absorbed from all beams under conventional irradiation conditions.

irradiation be all 48 beams. This map was plotted for the point in time 8.5 ns (the middle highest-power part of the pulse). As noted above, at each point (θ,φ) we selected the ρ^*/ρ_{cr} value of the beam with the greatest contribution to the energy deposition W. Since, according to Fig. 3a, the function W_1 peaks near the optical beam axis, the peaks (white areas) in the density (D^*) map coincide with the positions of the optical beam axes, i.e. show the target irradiation symmetry. As is clear in Fig. 5, the characteristic density $\rho^*(\theta,\varphi)$ is lower than the critical density and depends, like W and E, on angles θ and φ. This dependence makes a contribution to the non-uniformity of ablation pressure in the target. To estimate the effect of W and ρ^* perturbations on the ablation pressure, advantage can be taken of the stationary corona model [8,9]. According to this model, the ablation pressure $p_{abl} = 2(2-f)\rho_s c_s^2$, where $f = 1.22$ is the factor, which defines the position of Jouguet point R_s relative to the ablation surface: $R_s = fR$. The model is characterised by the dimensionless parameter $\gamma_0 \sim Q/\rho_a^{7/4}$ (we take into account only the dependences on the laser flux Q and the density ρ_a, at which this flux is absorbed). According to Ref. [9], $\rho_s \sim \rho_a\gamma_0^{0.479}$ and $c_s \sim (1/\gamma_0^{0.214})(Q/\rho_a)^{1/3}$. Then the ablation pressure

$$p_{abl} = p_0\left(\frac{Q}{Q_0}\right)^{\alpha}\left(\frac{\rho_a}{\rho_{a0}}\right)^{\beta}, \qquad (16)$$

where p_0 is the spherically symmetric pressure for $Q = Q_0$ and $\rho_a = \rho_{a0}$; $\alpha = 0.718$; $\beta = 0.244$. When the flux Q and the density ρ_a exhibit deviations, $Q = Q_0 + \delta Q$ and $\rho_a = \rho_{a0} + \delta\rho_a$, for the ablation pressure perturbations we obtain:

$$\frac{\delta p_{abl}}{p_0} = \alpha\frac{\delta Q}{Q_0} + \beta\frac{\delta\rho_a}{\rho_{a0}}. \qquad (17)$$

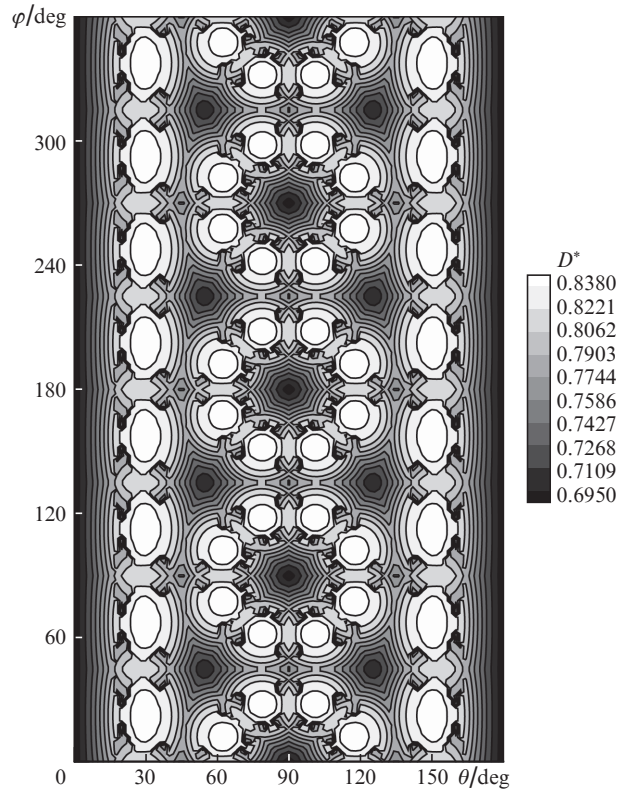

Figure 5. Map of the plasma density corresponding to the peak energy deposition under conventional irradiation conditions.

The ratio $\alpha/\beta = 2.94$, and therefore the ablation pressure deviations are 2.94 times more sensitive to flux deviations δQ than to density deviations $\delta\rho_a$.

The degree of absorbed flux uniformity depends on the ratio a/R of the beam radius at the target to the target radius. For a narrow beam the uniformity is lower but the absorbed fraction is higher. The fraction δ_a absorbed due to the inverse bremsstrahlung mechanism, the resonance absorption fraction δ_{ar} (of the incident laser energy) and the degree of uniformity η_E in relation to the ratio a/R are collected in Table 1 for $p = 2$ and $f = 0.06$. As follows from Table 1, with increasing a/R from 0.5 to 1.3 the absorbed fraction lowers from 0.755 to 0.465. In this case, the degree of uniformity rises from 0.9396 to 0.9741. It is noteworthy that, beginning with $a/R = 1$ and above, the degree of uniformity increases only slightly, while the absorbed fraction decreases. Since the resonance absorption fraction is very small (4.49×10^{-4} for $a/R = 1$), it was not taken into account in the calculations of absorbed flux uniformity. The low values of δ_{ar} are due to the large target dimension and, accordingly, the long plasma nonuniformity length in the vicinity of the critical point. In this case, only a very small fraction of the flux confined near the optical axis participates in the resonance absorption. For the Spitzer conductivity and $p = 2$ the absorption efficiency due to the inverse bremsstahlung is higher. For instance, for $a/R = 1$ we have $\delta_a = 0.754$, and it is higher for other a/R values, too. In this case, the degree of uniformity η_E changes slightly: for $a/R = 1$ it amounts to 0.9661 (versus 0.9663 in the case of limited thermal conduction). Also considered was the version with $p = 4$ and $f = 0.06$. The degree of uniformity hardly changes and amounts to 0.9661 for $a/R = 1$. The absorbed fraction is somewhat higher in this case and for $a/R = 1$ is equal to 0.642 (versus 0.57 for $p = 2$). This is because for $p = 4$, in comparison with $p = 2$, a part of the radiation with long impact parameters is 'transferred' to the domain of shorted impact parameters, for which the absorption efficiency is higher.

To determine the characteristic nonuniformity wavelengths for the angular distributions $E(\theta,\varphi)$, the deviations $\delta E = E - 1$ were expanded in spherical harmonic series:

$$\delta E(\mu,\varphi) = \sum_{k=0}^{L}\sum_{m=0}^{k} a_k^m Y_k^m(\mu,\varphi), \qquad (18)$$

where $Y_k^m(\mu,\varphi) = P_k^m(\mu)\exp(im\varphi)$; $P_k^m(\mu)$ are associated Legendre functions; a_k^m are expansion coefficients (complex quantities). Figure 6 shows the absolute values of the expansion coefficients $A_k^m = |a_k^m|$ in relation to number k for $m = 0$ (Fig. 6a) and $m = 1$ (Fig. 6b). One can see that the harmonic with $k = 8$ and $m = 0$ ($A_8^0 = 9.8\times10^{-3}$) is the leading harmonic. For $m > 1$ the coefficients A_k^m do not exceed the coefficient A_8^0. The greatest of them is coefficient $A_4^4 = 1.2\times10^{-5}$, which is smaller than A_8^0 by almost three orders of magnitude. The spherical harmonic expansion is usually used for investigating the linear stage of Rayleigh–Taylor instability. In the case of a shell target, which is under consideration here, this stage is 'forgotten' in the course of the shell's flight to the target centre. Since shell's velocity far exceeds the sound velocity in it, the shape of shell distortions prior to the onset of DT-substance compression is determined by the ballistics of different portions of the shell, which fly independently of each other. This approach was considered in Refs [1, 2, 11, 12].

Now let us consider the effects of different unconventional irradiation: beam energy disbalance, random misses of the beam axes relative to the target centre, and the target displacement from the common beam pointing centre. Figure 7a shows the dependence of beam energy on the beam number with the inclusion of random deviations according to Gaussian statistics with an error of $\varepsilon_b = 8\%$. Figure 7b shows the random scatter of the beam axis misses in the plane $\delta\cos\varphi_\delta, \delta\sin\varphi_\delta$, where δ is the axis miss relative to the target centre and φ_δ is the angle measured in the XY plane relative to the X axis. The miss distance δ is defined by the Gaussian random number distribution with a characteristic value δ_0 (shown in Fig. 7b is the case $\delta_0 = 160$ μm), with a uniform distribution in angle φ_δ. We note that the positions of points in Fig. 7b are not the positions of the axes in the XY plane, since the distance of the origin from a point in the XY plane is greater than the miss distance due to the beam axis inclination relative to the XY plane. The values of the degree of nonuniformity η_E and the difference between the maximum and the minimum $\varepsilon_E = 1 - \eta_E$

Table 1.

Parameter	a/R								
	0.5	0.6	0.7	0.8	0.9	1.0	1.1	1.2	1.3
δ_a	0.755	0.722	0.686	0.648	0.609	0.570	0.533	0.498	0.465
δ_{ar}	2.44×10^{-3}	1.60×10^{-3}	1.10×10^{-3}	7.93×10^{-4}	5.86×10^{-4}	4.49×10^{-4}	3.57×10^{-4}	2.93×10^{-4}	2.45×10^{-4}
η_E	0.9396	0.9593	0.9566	0.9525	0.9554	0.9663	0.9678	0.9725	0.9741

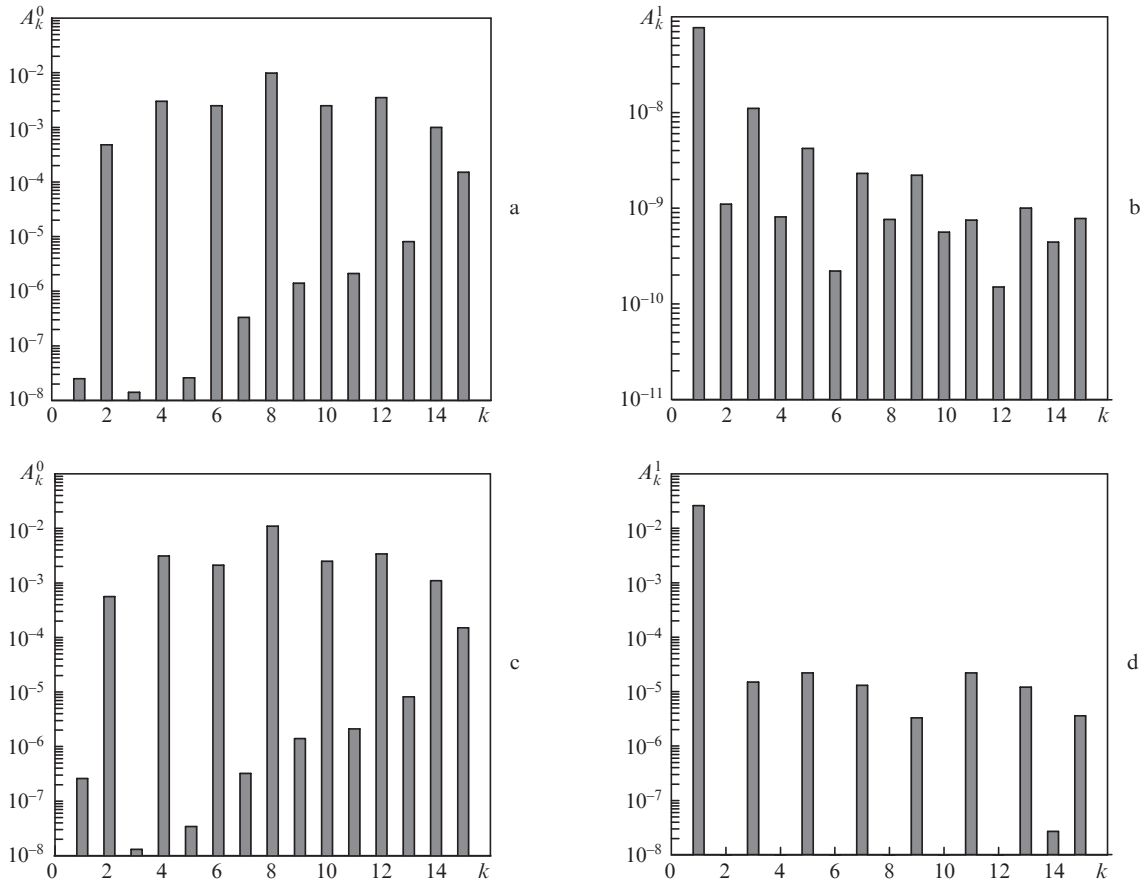

Figure 6. Spherical harmonic expansion coefficients for the deviation of absorbed energy distribution function from the average value (a, b) under conventional irradiation conditions and (c, d) for a target displacement by 80 μm along the X axis. Given are the dependences on harmonic number k for m = (a, c) 0 and (b, d) 1.

for different disbalance values ε_b are collected in Table 2. From Table 2 it follows that disbalance growth by 8% results in an increase in nonuniformity ε_E by only 1%. This low responsivity of the nonuniformity to the disbalance of beam energies is attributable to the fact that eight significantly overlapping beams are incident on the target from the side of each cube face, and the difference in the total energy of each of these six beam groups is approximately eight times smaller than the difference of separate beam energies. This merely confirms the high quality of the random number sample used

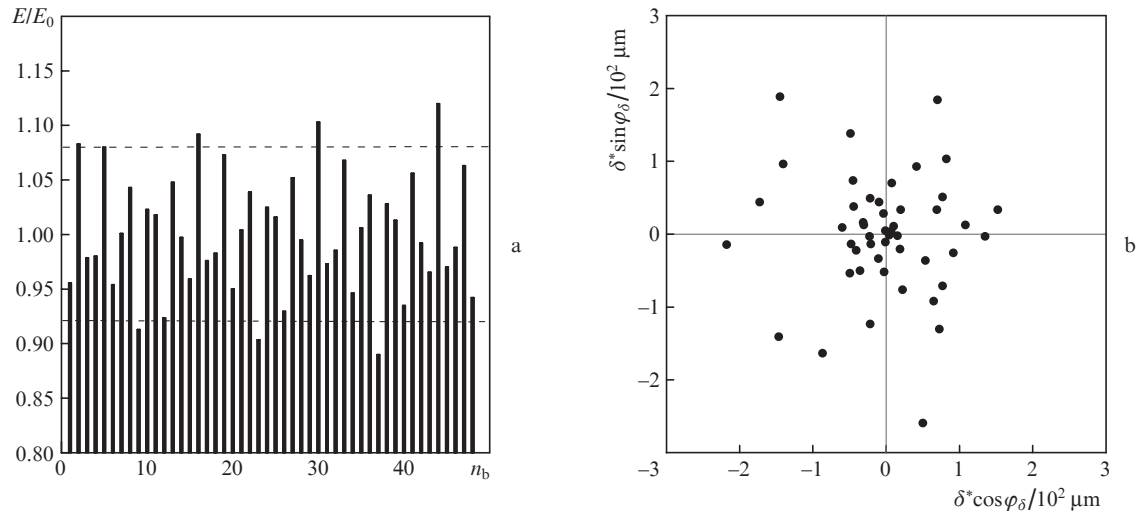

Figure 7. (a) Dependence of the pulse energy on its number for the Gaussian statistics of random deviations from the average value (the characteristic deviation ε_b = 8%, dashed lines show the 8% range) and (b) random scatter of beam axis miss distances relative to the target centre for the Gaussian statistics of the miss distance δ with the characteristic value δ_0 = 160 μm and the uniform statistics of the angle φ_δ measured in the XY plane relative to the X axis.

Table 2.

Parameter	ε_b (%)			
	0	4	8	16
η_E	0.9663	0.9612	0.9562	0.9462
ε_E (%)	3.37	3.88	4.38	5.38

Table 3.

Parameter	δ_0/R (%)		
	5	10	20
η_E	0.9501	0.9321	0.8864
ε_E (%)	4.99	6.79	11.36
Δ_a	0.568	0.566	0.562

Table 4.

Parameter	D/R (%)		
	2.5	5	10
ε_{EX} (%)	7.87	12.86	20.60
ε_{EXY} (%)	7.12	10.89	18.88
ε_{EXYZ} (%)	6.89	11.08	19.46

to determine the beam energy spread. Collected in Table 3 are the values of η_E and ε_E for different δ_0 values and random beam axis misses depicted in Fig. 7b ($\delta_0 = 160$ μm corresponds to $\delta_0/R = 10\%$). In the variation of δ_0, use was made of the same random beam distribution depicted in Fig. 7b, the family of points was only expanded or compressed in the radial direction. Also given in Table 3 are the absorbed fractions Δ_a for different δ_0/R ratios, whence it follows that the effect on Δ_a produced by the beam misses under consideration may be neglected. Table 4 gives the values of ε_E for different absolute values of target displacement from the common beam pointing centre D/R and its three directions: ε_{EX} for a displacement along the X axis; ε_{EXY} for a displacement in the XY plane, whereby the displacement direction makes equal angles with X and Y axes; ε_{EXYZ} for a displacement between the X, Y, and Z axes, whereby the displacement direction makes equal angles with the X, Y, and Z axes. From Tables 2–4 it follows that the nonuniformity of absorbed energy is most sensitive to the target displacement from the common centre. In this case the relative nonuniformity ε_E is approximately two times greater than the relative displacement. This is attributable to the following fact: in the displacement of the target, one of its sides enters the zone of higher irradiance, while the other side, by contrast, leaves it, which makes a double contribution to the increase in nonuniformity. Among the three unconventional irradiation cases, the case of beam misses occupies an intermediate position from the standpoint of increasing the nonuniformity (for a 10% miss, $\varepsilon_E = 6.79\%$).

The angular absorbed energy distributions $E(\theta,\varphi)$ for the three unconventional irradiation cases considered above are depicted in Figs 8–10: for beam energy disbalance in Fig. 8 for $\varepsilon_b = 8\%$, for random beam misses for $\delta_0/R = 10\%$ in Fig. 9, for the target displacement along the X axis in Fig. 10 for $D/R = 5\%$. In the case of beam energy disbalance the angular distribution is little different from the case of conventional irradiation (see Fig. 4). A special feature of $E(\theta,\varphi)$ in the case of random beam misses is the appearance of low modes in the distribution function. The reason is that owing to the Gaussian distribution of miss distances δ the point density in Fig. 7b, which characterises these misses, is maximal

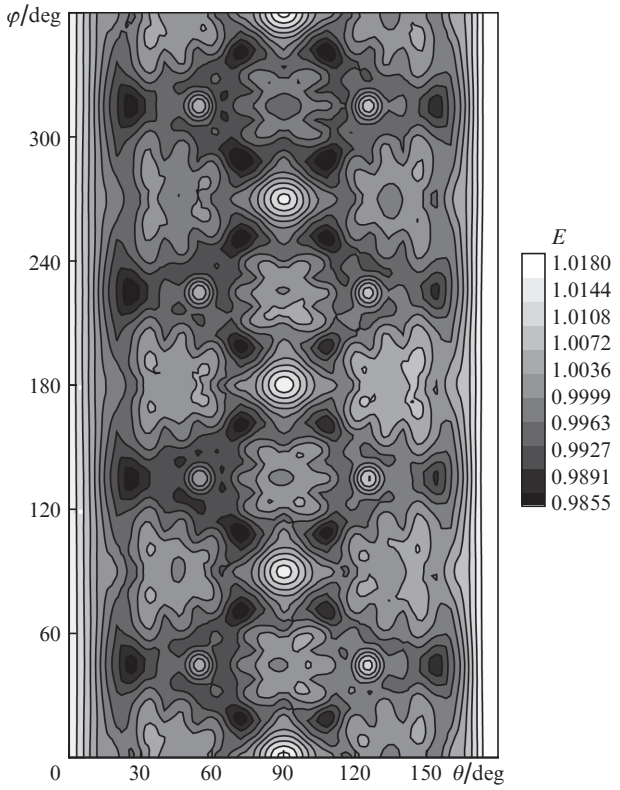

Figure 8. Angular distribution function for absorbed energy for a beam energy disbalance with a characteristic deviation $\varepsilon_b = 8\%$.

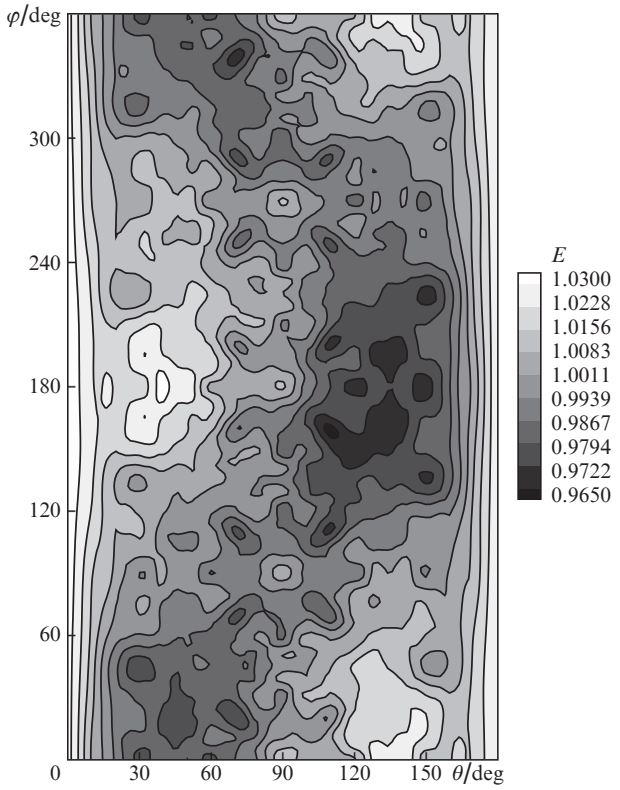

Figure 9. Angular distribution function for the energy absorbed in the case of random beam misses with a characteristic ratio $\delta_0/R = 10\%$.

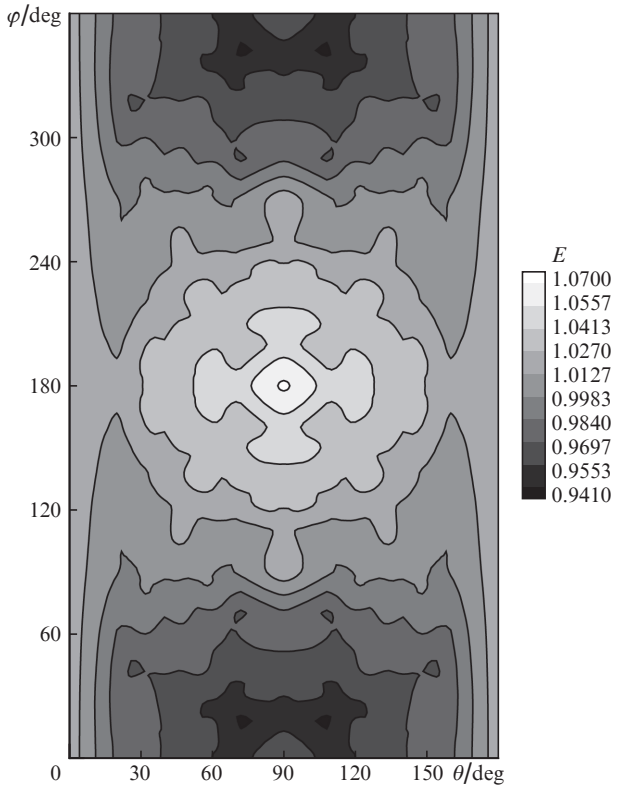

Figure 10. Angular distribution function for the energy absorbed in the case of target displacement from the beam pointing centre by 80 μm (5% of the target radius) along the X axis.

at the drawing centre and lowers with increasing δ. In this case, only a small number of beams exhibit large misses, which results in the appearance of low modes in the $E(\theta,\varphi)$ distribution. When the target is displaced from the common beam pointing centre, there appears the first harmonic in the $E(\theta,\varphi)$ distribution. Figures 6c and 6d show the absolute values of coefficients $A_k^m = |a_k^m|$ in expansion (18) for the distribution depicted in Fig. 10 (target displacement). This drawing suggests that the harmonic with $k = 1$, $m = 1$ is the leading one.

The angular absorbed flux distributions $W(\theta,\varphi,t)$ obtained in the present work were employed for one- and two-dimensional simulations of compression and burning of a laser fusion target [1, 2, 11, 12]. These simulations made it possible to determine the measure of lowering of the fusion target gain under the above irradiation conditions in comparison with the case of spherically symmetric compression.

4. Conclusions

We have proposed a physicomathematical model for calculating the angular distribution of absorbed laser flux in the corona of a spherical target with the inclusion of radiation refraction. Considered by way of example is the target irradiation geometry of cube symmetry corresponding to a megajoule laser facility. Under conventional irradiation conditions, when the energies of all beams are equal and their axes pass through the target centre, the difference between the maximum and minimum of the angular distribution function of absorbed energy amount to 3.37%. In this case, the leading spherical harmonic is the harmonic with $k = 8$ and $m = 0$. Several versions of unconventional irradiation were considered: when the beams have a random energy spread (disbalance), when the optical beam axes randomly miss the target centre, and when the target is displaced relative to the centre of beam pointing. The smallest uniformity impairment appears in the case of beam energy disbalance. A disbalance of 8% impairs the uniformity by about 1%. The case of beam misses occupies an intermediate position. For a characteristic miss distance of 10% of the target radius the nonuniformity increases by 3.42% in comparison with conventional conditions. The most severe impairment of uniformity occurs when the target is displaced from the beam pointing centre. When the target is displaced along the X axis by a distance of 5% of the target radius, the nonuniformity increases by 9.49%. In this case, in the angular distribution function for the absorbed flux the first harmonic in angle φ ($k = 1$, $m = 1$) has the highest amplitude.

Acknowledgements. This work was supported by the Russian Science Foundation (Grant No. 16-11-10174).

References

1. Bel'kov S.A., Bondarenko S.V., Vergunova G.A., et al. *JETP*, **121**, 686 (2015) [*Zh. Eksp. Teor. Fiz*., **148**, 784 (2015)].
2. Bel'kov S.A., Bondarenko S.V., Vergunova G.A., et al. *JETP*, **124**, 341 (2017) [*Zh. Eksp. Teor. Fiz*., **151**, 396 (2017)].
3. Danilov A.E., Demchenko N.N., Rozanov V.B., et al. *Sov. J. Quantum Electron*., **7**, 579 (1977) [*Kvantovaya Elektron*., **4**, 1034 (1977)].
4. Howard J.E. *Appl. Opt*., **16**, 2764 (1977).
5. Volenko V.V., Kryuchenkov V.B. *Sov. J. Quantum Electron*., **9**, 789 (1979) [*Kvantovaya Elektron*., **6**, 1343 (1979)].
6. Scannapieco A.J., Brysk H. *J. Appl. Phys*., **50**, 5142 (1979).
7. Rozanov V.B., Demchenko N.N. *Sov. J. Quantum Electron*., **15**, 1251 (1985) [*Kvantovaya Elektron*., **12**, 1895 (1985)].
8. Afanas'ev Yu.V., Gamalii E.G., Krokhin O.N., Rozanov V.B. *JETP*, **44**, 311 (1976) [*Zh. Eksp. Teor. Fiz*., **71**, 594 (1976)].
9. Afanasiev Yu.V., Gamaly E.G., Gus'kov S.Yu., et al. *Las. Part. Beams*, **6**, 1 (1988).
10. Afanas'ev Yu.V., Gamalii E.G., Demchenko N.N., et al. *JETP*, **52**, 425 (1980) [*Zh. Eksp. Teor. Fiz*., **79**, 837 (1980)].
11. Demchenko N.N., Doskoch I.Ya., Gus'kov S.Yu., et al. *Las. Part. Beams*, **33**, 655 (2015).
12. Gus'kov S.Yu., Demchenko N.N., Zmitrenko N.V., et al. *JETP Lett*., **105**, 402 (2017) [*Pis'ma Zh. Eksp. Teor. Fiz*., **105**, 381 (2017)].